# Response of Sm-Nd isotope systematics to complex thermal histories: A case study from 3.58 Ga gneisses of the Pilbara Craton

Andreas Petersson, Anthony I. S. Kemp, Maud Boyet, Martin J. Whitehouse, Matilda Boyce, Malcolm Roberts, Allen Kennedy

Earth and Planetary Science Letters 620 (2023) 118346

Contents lists available at ScienceDirect

Earth and Planetary Science Letters

journal homepage: www.elsevier.com/locate/epsl

# Response of Sm–Nd isotope systematics to complex thermal histories: A case study from 3.58 Ga gneisses of the Pilbara Craton

Andreas Petersson [a,b,c,*], Anthony I.S. Kemp [a], Maud Boyet [d], Martin J. Whitehouse [c], Matilda Boyce [a], Malcolm Roberts [a], Allen Kennedy [e]

[a] School of Earth Sciences, The University of Western Australia, Crawley, Australia
[b] Department of Geography and Geology, University of Copenhagen, Øster Voldgade 10, DK-1350 Copenhagen K, Denmark
[c] Swedish Museum of Natural History, Box 50 007, SE-104 05 Stockholm, Sweden
[d] Université Clermont Auvergne, CNRS, IRD, OPGC, Laboratoire Magmas et Volcans, F-63000 Clermont-Ferrand, France
[e] John de Laeter Center, Curtin University, Perth, Western Australia 6845, Australia

ARTICLE INFO

*Article history:*
Received 24 March 2023
Received in revised form 25 July 2023
Accepted 4 August 2023
Available online xxxx
Editor: F. Moynier

*Keywords:*
in situ Sm-Nd isotopes
zircon U-Pb-O-Hf isotopes
Archean
allanite
Pilbara

ABSTRACT

In felsic igneous rocks, the parent and daughter elements in the widely used Sm–Nd and Lu–Hf isotope tracer systems are mainly hosted in accessory phases. Recrystallisation and/or breakdown of these minerals during metamorphism, deformation and weathering potentially compromises the chemical and isotopic composition of the respective whole rocks, impeding the utility of such information for deducing the timing, rates and processes of crust-mantle differentiation in the early Earth. The different abilities of zircon and REE-rich minerals to withstand metamorphism have been suggested as a reason for the decoupling of the Lu–Hf and Sm–Nd isotope systems observed in a number of ancient gneiss terranes. The controls on element mobility and subsequent isotopic disturbance during recrystallisation and breakdown of LREE-rich accessory minerals are, however incompletely understood. Here, we use petrography, element mapping, and microanalysis of accessory minerals, in tandem with whole rock Sm–Nd data, to assess the reliability of the Sm–Nd system in the 3.59–3.58 Ga Mount Webber Gabbros, the oldest rocks in the Pilbara Craton (Western Australia). We show that despite multiple thermal events, which reset the mineral Sm–Nd systematics, and decomposition of the REE-rich mineral allanite, the Mount Webber rocks retained the Sm–Nd isotope signatures of their magmatic protoliths at the whole-rock scale. We show that the allanite breakdown occurred during modern, near-surface weathering processes at low temperature, such that the REE were sequestered into secondary minerals rather than escaping in higher temperature metamorphic fluids. The whole rock Sm–Nd, and zircon O–Hf signatures, together with new $^{142}$Nd isotope data, suggest derivation of the Mount Webber rocks from undifferentiated mantle sources that preserve no evidence for Hadean silicate Earth differentiation. This study highlights the benefits of a combined analytical approach using both in-situ and whole-rock isotope analyses to obtain a more complete record of the source and thermal evolution of ancient, highly metamorphosed igneous rocks.



## 1. Introduction

Radiogenic and stable isotope systems have long been important tools for studying the evolution of the continental crust. Of these, the whole-rock $^{147}$Sm–$^{143}$Nd isotope system continues to be one of the most important and widely used tracers of crustal growth and mantle depletion (e.g. Allègre and Rousseau, 1984; DePaolo et al., 1991). However, Archean rocks commonly comprise polyphase metamorphic gneiss terranes, and the reliability of the Sm–Nd isotope signatures of ancient rocks has been questioned, particularly regarding whether the parent/daughter ratio of the original igneous rock has been modified, and thus whether accurate initial isotope compositions can be obtained (e.g., Vervoort et al., 1996; Hammerli et al., 2019). The similar geochemical behaviour of Sm and Nd has been used to argue against differential Sm and Nd mobility during post-magmatic disturbance, and the fidelity of the Sm–Nd isotope system has been claimed in Precambrian and even some Archean terranes (DePaolo et al., 1991; Bennett, 2003).

* Corresponding author at: Department of Geography and Geology, University of Copenhagen, Øster Voldgade 10, DK-1350 Copenhagen K, Denmark.
*E-mail address:* ape@ign.ku.dk (A. Petersson).

https://doi.org/10.1016/j.epsl.2023.118346

Whole-rock Nd isotope ratios of some early Archean rocks are super-chondritic at the protolith crystallisation age, which has been interpreted to suggest crustal separation from a depleted mantle source (e.g., Bowring and Housh, 1995). In contrast, zircon and whole-rock Hf isotope signatures from Eoarchean meta-igneous rocks on a number of different continents are compatible with a near-chondritic mantle composition (Fisher and Vervoort, 2018; Petersson et al., 2020; Kemp et al., 2023). The correlation between the whole-rock Sm–Nd and the zircon Lu–Hf system, which is strong throughout most of Earth's history (Vervoort et al., 2011), therefore breaks down in the ancient rocks from polymetamorphic terranes. This Hf–Nd isotope 'decoupling' is observed in data from southern West Greenland (e.g. Rizo et al., 2011; Kemp et al., 2019; Hammerli et al., 2019), the Acasta Gneiss Complex (Bauer et al., 2017; Fisher et al., 2020) and from the oldest rocks from the Kaapvaal Craton (Schoene et al., 2009; Zeh et al., 2011). Non-correlated Hf–Nd isotope systematics are also reported from younger rocks, such as Hercynian (∼0.32 Ga) leucogranites from the French Massif Central (Luais et al., 2009).

The Hf–Nd isotope decoupling, especially in ancient gneisses, has been attributed to early differentiation processes deep in the silicate Earth (Hoffmann et al., 2011; Rizo et al., 2011). Another explanation is that the Hf–Nd isotope discrepancy reflects REE mobility during metamorphism (e.g., McCulloch and Black, 1984), perhaps due to reactions involving REE-rich accessory minerals (Hammerli et al., 2019; Fisher et al., 2020). More than 90% of the Hf in granitic rocks is typically hosted by zircon, while the REE-rich accessory minerals allanite, apatite and epidote are the main repositories of LREE in felsic to intermediate rocks, and may host >75% of the Nd budget in such samples (Hammerli et al., 2019). However, the ability of zircon to withstand metamorphism and alteration and retain a primary chemical signature is greater than that of allanite, epidote, titanite and apatite (Scherer et al., 2000). This opens up the possibility of Nd mobility within a whole rock that has retained a closed zircon Lu–Hf system. Hammerli et al. (2019) suggest that open-system processes, mobilising and fractionating Sm and Nd, can lead to disturbance of whole-rock Nd isotope systematics. Hence, while igneous zircon preserves the Hf isotopic composition of the crystallizing magma, the whole rock initial $^{143}Nd/^{144}Nd$ signature may not be that of the magma from which the rock formed (Luais et al., 2009; Kemp et al., 2019; Hammerli et al., 2019; Fisher et al., 2020; Wang et al., 2022). In the case of leucogranites from the French Massif Central, Luais et al. (2009) show that even the least deformed samples in their study have decoupled Sm–Nd and Lu–Hf systems as a result of elevated Sm/Nd induced by fluid mobilization, without fractionation of Lu/Hf. These authors also show a resolvable change towards higher $\varepsilon_{Nd(t)}$ at constant $\varepsilon_{Hf(t)}$ with increasing deformation. It should be noted that metamorphic disturbance of Lu/Hf in Mg-rich rocks (e.g., boninites) has been proposed as a reason for Nd–Hf decoupling (Carlson et al., 2019), but as this notion is based on whole-rock Lu–Hf it still fails to explain the discrepancy between zircon Lu–Hf and whole-rock Sm–Nd.

One way to assess the reliability of a whole rock initial Nd isotope ratio is to compare the independently obtained magmatic crystallisation age (e.g., from U–Pb in zircon) with the date obtained from a Sm–Nd isochron defined by the accessory phases that control the Sm–Nd budget of that particular rock (e.g., Hammerli et al., 2019; Fisher et al., 2020; Salerno et al., 2021; Wang et al., 2022). Agreement between these dates would constitute strong evidence that the Nd isotope system has remained closed since the rock formed (Salerno et al., 2021). This approach has been utilized in high-grade gneiss terranes in southwest Greenland (Hammerli et al., 2019) and the Acasta Gneiss Complex (Fisher et al., 2020), and also in the much better-preserved granite-greenstone terranes of the Pilbara Craton (Salerno et al., 2021). Salerno et al. (2021) showed that 3.47 to 3.28 Ga granitic rocks of the Mount Edgar Granitic Complex retained a closed Nd isotope system and have chondritic signatures for both Hf (zircon) and Nd (titanite and apatite). It is notable, however, that at 3.47 Ga, whole rock $\varepsilon_{Nd}$ values of Pilbara felsic igneous rocks range from −1.5 to +2 (Gardiner et al., 2017; Kemp et al., 2023). The causes of this $\varepsilon_{Nd}$ spread, particularly whether this reflects source heterogeneity or isotope disturbance, requires further investigation.

In this study, we test the reliability of the whole-rock Sm–Nd isotope system in Archean rocks by examining the 3.59–3.58 Ga Mount Webber Gabbro and associated granitic gneisses of the northeastern Pilbara Craton. These are the oldest rocks in the craton, and show evidence for pervasive deformation and amphibolite facies metamorphism (Petersson et al., 2019a). The Mount Webber samples yield zircon Hf–O isotope signatures in line with generation from a chondritic source (Petersson et al., 2019a), although the Nd isotope characteristics of these rocks are unknown. We report Nd isotope compositions of REE-rich accessory minerals (allanite, titanite, apatite and scheelite) in these gabbro samples, determined by microanalysis, and present new whole-rock $^{146-147}Sm$–$^{142,143}Nd$ data. We also report rutile U–Pb data and zircon U–Pb, O and Lu–Hf data for these rocks to provide a broader framework for interpretation of the Sm–Nd isotope data, and to allow the magmatic source and metamorphic history of this region to be reconstructed. The data reveal a coupled Nd–Hf isotope system that in combination with zircon O isotopes suggest derivation of the Mount Webber samples from a primitive, undifferentiated mantle source. The data also show that the Mount Webber rocks retained their Sm–Nd isotope integrity at the scale of sampling, despite variable metamictisation, breakdown and Sm–Nd isotope resetting of the constituent REE-rich minerals during a number of post-crystallisation thermal events. This study highlights the benefits of a combined analytical approach using both in-situ and whole-rock isotope analyses to obtain the clearest picture of the source and evolution of ancient metamorphosed igneous rocks.

## 2. Geological setting

The samples in this study were collected from the oldest magmatic unit of the Pilbara Craton, located in the northwestern part of the Shaw Granitic Complex in the East Pilbara Terrane (a more detailed geological description of the Pilbara Craton is provided in Appendix A-1). The type area of the Mount Webber gabbro extends over 500 × 300 metres. It comprises a diverse assemblage of gabbroic, leucogabbroic, dioritic and tonalitic gneisses that crop out together with small pods of highly altered ultramafic rock (Fig. 1; Petersson et al., 2019a). A weakly porphyritic granodiorite occurs immediately to the north, but no clear contact between this lithology and the gabbroic-leucogabbroic gneisses has been found. The southern part of the outcrop area is dominated by gneissic diorite to tonalite, which is interspersed with discontinuous strips of intensely deformed, banded leucogranitic gneiss.

The gabbroic to leucogabbroic rocks are heterogeneous on an outcrop scale both in terms of grain size and mineralogy, but the dominant variety is a coarse-grained, rutile-bearing leucogabbro dated at 3.58 Ga (zircon U–Pb, Petersson et al., 2019a). Hornblende-rich metagabbros, locally with diffuse layering of mafic minerals, occur as several conspicuous lenses up to 40 metres long (Petersson et al., 2019a). One of these gabbros returned a zircon U–Pb age of ca. 3.43 Ga (Petersson et al., 2019a), very similar to the magmatic crystallisation age of a granodiorite cropping out ∼2 km to the north (3.43 Ga, SHRIMP, U–Pb in zircon; McNaughton et al., 1993). Zegers et al. (1999) report Ar–Ar (hornblende) plateau dates of 3.006 ± 0.0011 Ga for a mylonitic granodiorite and 3.038 ± 0.0011 Ga for a foliated amphibolite enclave 250–300 metres southwest of the leucogabbros. These dates are

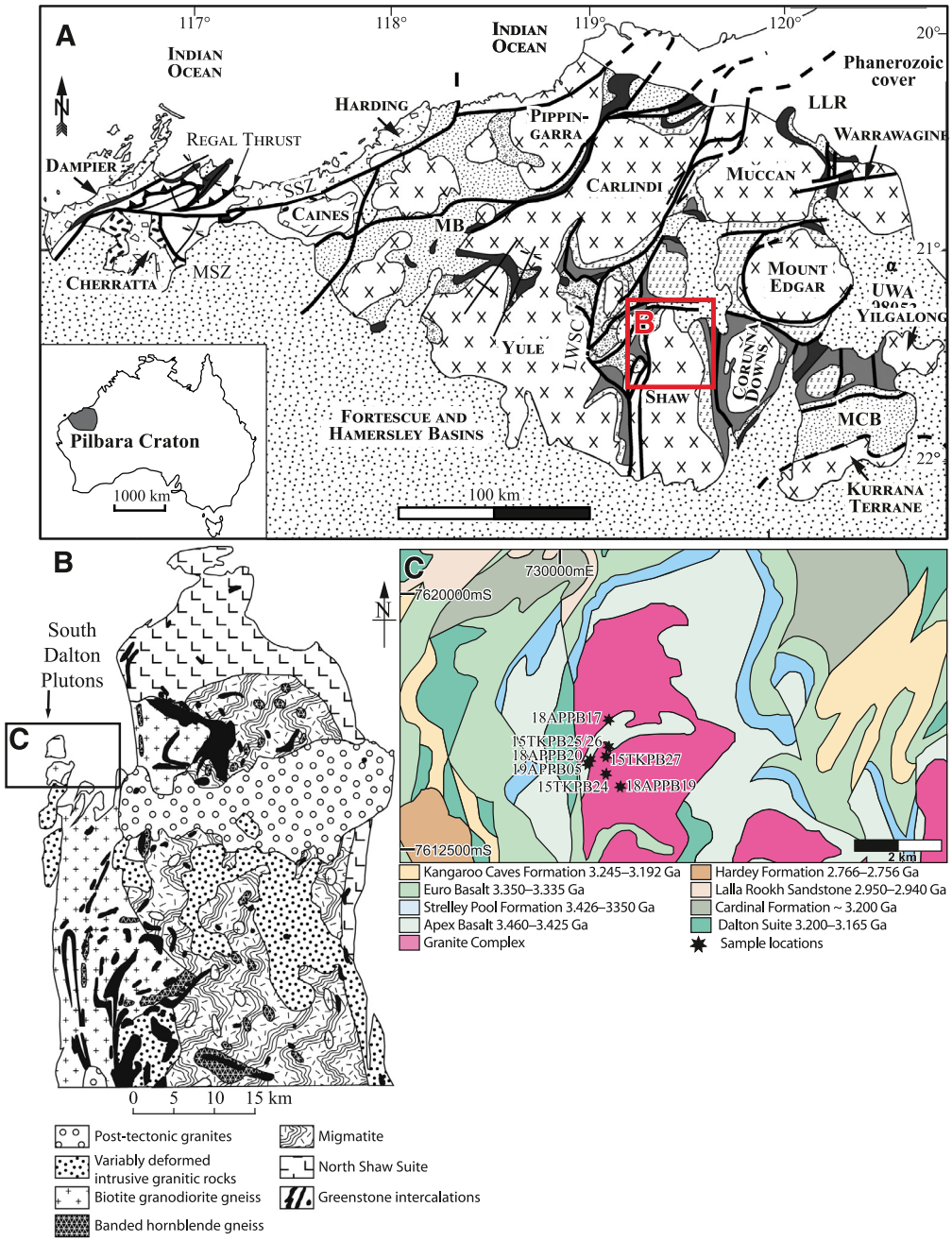


**Fig. 1.** A) Simplified geological map of the Pilbara Craton in Western Australia (modified after Kemp et al., 2015). LWSC = Lalla Rookh–Western Shaw structural corridor; MB = Mallina Basin; MCB = Mosquito Creek Basin; MSZ = Maitland Shear Zone; SSZ = Sholl Shear Zone. Red square denoted location of B. B) Simplified geology of the Shaw Granitic Complex. Modified after Bickle et al. (1983). C) The Mount Webber and surrounding area showing sample locations and the proximity of the Kangaroo Caves Formation to the sample locality.

interpreted as cooling ages from a deformational event that preceded the development of the Mulgandinnah Shear Zone (MSZ), a craton-scale strike slip zone that occurs along the western margin of the Shaw Granitic Complex, ca. 10 kilometres east of the Mount Webber area. A minimum age of ca. 2.94 Ga has been established for amphibolite facies metamorphism associated with activity on the MSZ (Zegers et al., 1999).

## 3. Methods

### 3.1. Sampling strategy

Four new samples were collected from the Mount Webber Gabbro type locality, to encapsulate the range of lithologies in this area (Fig. 1, Appendix A-1). Two different samples of the dioritic to tonalitic gneiss were collected, one texturally homogeneous (15TKPB24) and the other having a clotty texture of mafic minerals with larger hornblende crystals (18APPB19). A leucogranitic gneiss, enclosed by dioritic to tonalitic gneisses in the southern part of the area (18APPB20, 19APPB05), and a weakly porphyritic granodiorite (18APPB17) were also sampled. Petrographic descriptions are included in Appendix A-1.

### 3.2. Analytical methods

Analytical methods are detailed in Appendix A-1, and are summarised below.

*3.2.1. REE-bearing minerals*

Polished thin sections were studied by optical microscopy and Scanning Electron Microscopy (SEM) at the Centre of Microscopy, Characterisation and Analysis (CMCA), University of Western Australia. Electron Probe Micro-Analysis (EPMA) was used to determine the composition of allanite grains in three samples (15TKPB24, 15TKPB27 and 18APPB19). Accessory minerals, including apatite, titanite, allanite and scheelite, from four different rocks (15TKPB24, 15TKPB25, 15TKPB27 and 18APPB19) were subsequently analysed in-situ for Sm–Nd isotopes (Appendix Table A-2). Data were obtained from 60 µm thick polished thin sections and one grain-mount using a 193 nm Cetac Analyte G2 excimer laser coupled to a Thermo Scientific Neptune Plus in the CMCA (see Hammerli et al., 2019).

*3.2.2. Zircon and rutile*

Zircon grains extracted from samples 15TKPB24, 18APPB17 and 18APPB20 were U–Pb dated by secondary ion mass spectrometry (SIMS), using a Cameca IMS1280 at the Swedish Museum of Natural History (Appendix Table A-3; see Whitehouse et al., 1999, and Whitehouse and Kamber, 2005). Rutile grains were separated from samples 15TKPB25, 15TKPB26 and 15TKPB27, the zircon crystals of which were previously U–Pb dated (SIMS) to ca. 3.58 Ga (Petersson et al., 2019a). The rutile was analysed for U–Pb isotopes (Appendix Table A-4) by SHRIMP II at the John de Laeter Centre, Curtin University, following the methodology of Taylor et al. (2012). Rutile was targeted because the grains are coarse and well preserved in the samples, and because its U–Pb systematics can give insight into the thermal history of the area (e.g., Smye et al., 2018). All weighted mean U–Pb ages are reported at 95% confidence.

Following U–Pb analysis, oxygen isotope ratios ($^{18}O/^{16}O$) in zircons of samples 15TKPB24, 18APPB17 and 18APPB20 (Appendix Table A-5) were determined using a Cameca IMS 1280 ion microprobe in the CMCA, following protocols described in Petersson et al. (2020). Zircon grains in samples 15TKPB24, 18APPB17 and 18APPB20 (Appendix Table A-6) were then analysed for Hf isotopes using the same instrumentation as for the in situ Sm–Nd analysis. Weighted mean zircon $\delta^{18}O$ and $\varepsilon_{Hf}(t)$ values are reported at 95% confidence limits.

*3.2.3. Whole rock Sm–Nd isotope analysis*

$^{147}Sm$–$^{143}Nd$ isotope data are reported for samples 15TKPB24, 15TKPB25 and 15TKPB27, 18APPB19, 18APPB20 as well as 19APPB05, all of which are assigned protolith crystallisation ages of 3.58 Ga (Appendix A-1). The $^{147}Sm/^{144}Nd$ values were obtained by isotope dilution techniques and measured on the Neptune Plus MC-ICPMS in the Laboratoire Magmas et Volcans. The Nd isotope ratios were measured by thermal ionisation mass spectrometry (Triton) using a two mass-step acquisition scheme, as outlined by Guitreau et al. (2019). High precision $^{142}Nd/^{144}Nd$ ratios were obtained for samples 15TKPB24, 15TKPB25, 18APPB19, 18APPB20 and 19APPB05 (Appendix, Table A-7).

## 4. Results

### 4.1. Occurrence and chemistry of LREE-rich accessory minerals

Photomicrographs showing the textural context of accessory minerals are presented in Appendix A-8. Apatite forms small, generally unaltered granules in all samples, occurring at grain boundaries and as inclusions in all major phases. Rutile forms aggregates of crystals in the gabbroic rocks (15TKPB25, 15TKPB26, 15TKPB27; see Petersson et al., 2019a), whereas titanite occurs in the diorite-tonalitic samples as anhedral grains in the groundmass and polycrystalline aggregates that in part form coronas around ilmenite (Appendix A-8). Scheelite (identified by EDS spectra) occurs as trails of colourless blebs in dioritic gneiss 18APPB19.

In all samples, allanite is most conspicuous as small brownish prisms surrounded by dark radiation haloes in hornblende. Upon close examination, these allanite grains have weakly birefringent, microcrystalline centres that are fringed by epidote, in some cases preserving the crystal outline. These features suggest metamictisation and alteration of the original allanite grains. This heterogeneity is clearly evident in back-scattered electron (BSE) images and is reflected in the element distribution, especially for the REEs (Figs. 2–3). Almost all former allanite grains can be divided into three different microstructural domains, BSE bright white, BSE light grey and BSE dark grey (see Appendix A-9). The bright white domains commonly occur as thin strips or irregular patches located in the central parts of the grains, and can be further divided into uniform and spongy-textured. The BSE dark grey material has a grainy texture and makes up the central part of the grains, whereas the BSE light grey material occurs as both core domains and as concentric rims mantling the composite grains.

The uniform BSE bright domains are compositionally akin to monazite, with high REE (LREE > 50%), Th (4.8-11.9% $ThO_2$) and $P_2O_5$ (ca. 27-28 wt.%) (Appendix A-9, see also Figs. 2 and 3). The spongy-textured domains are also very REE-rich (55-70% LREE) and have elevated Th (1.5-5.7% $ThO_2$), but are variable from grain to grain for Si, Al and Ca; F is up to 3.8%, but P is below detection. Low EPMA totals (76-82%) probably reflect the porous nature and presence of volatiles in these spongy domains, together with the irregular topography of the polished grain surface. The composition of the BSE dark areas varies strongly from spot to spot, which is probably a function of the finely polycrystalline and highly fractured nature of this material; LREE contents are generally 2–3%, besides one spot that has ~20% LREE (18APPB19 A8-005; Appendix 9). The BSE light grey domains appear to comprise epidote-group minerals, as suggested by the petrography, that vary from REE-poor (e.g., spots A8-3 and A8-4 in 18APPP19, with < 0.5% LREE but ca. 37.5% $SiO_2$, 25% $Al_2O_3$ and 21% CaO) to REE-rich (e.g., spot A1-7 in 15TKPB27, with ca. 16% LREE and 36% $SiO_2$, 19.3% $Al_2O_3$ and 12.5% CaO).

Regarding Sm/Nd, within a single composite allanite grain, the BSE-bright spongy domains have slightly lower Sm/Nd (ca. 0.04) than the uniform BSE-bright domains (0.06-0.07) and the light grey material. Overall, the BSE-bright and BSE-grey material have a large and overlapping spread of Sm/Nd (see Appendix A-10). All Sm/Nd values are significantly lower than those of the corresponding whole rocks (Sm/Nd ~0.18-0.20)

### 4.2. Zircon U–Pb, O–isotope and Lu–Hf data of felsic rocks

*4.2.1. 15TKPB24 tonalitic gneiss*

Small, low quality zircon grains were recovered from this sample. The U–Pb analyses are mostly discordant and yield a complex spread in $^{207}Pb/^{206}Pb$ dates from 3.60 to 2.24 Ga. There is a clear correlation between $^{207}Pb/^{206}Pb$ date and concordance, where concordance increases with age, indicating Pb loss (Fig. 4). The <10% discordant analyses have a spread of $^{207}Pb/^{206}Pb$ dates between 3.6 and 3.52 Ga. The seven oldest of these $^{207}Pb/^{206}Pb$ dates return a weighted mean age of 3.576 ± 0.014 Ga (MSWD = 10.8, Appendix Table A-3).

Nine O isotope analyses in five grains exhibit $\delta^{18}O$ values between 4.2 and 5.6‰, with a weighted mean of 5.2 ± 0.4‰ (MSWD = 0.6; Fig. 5; Appendix Table A-5). Five analyses for Lu–Hf isotopes yield $^{176}Hf/^{177}Hf$ ranging between 0.28049 and 0.28071 corresponding to $\varepsilon_{Hf(3.576Ga)}$ from −0.7 to +0.5 with a weighted mean of −0.2±0.4 (MSWD = 0.6, Appendix Table A-6).

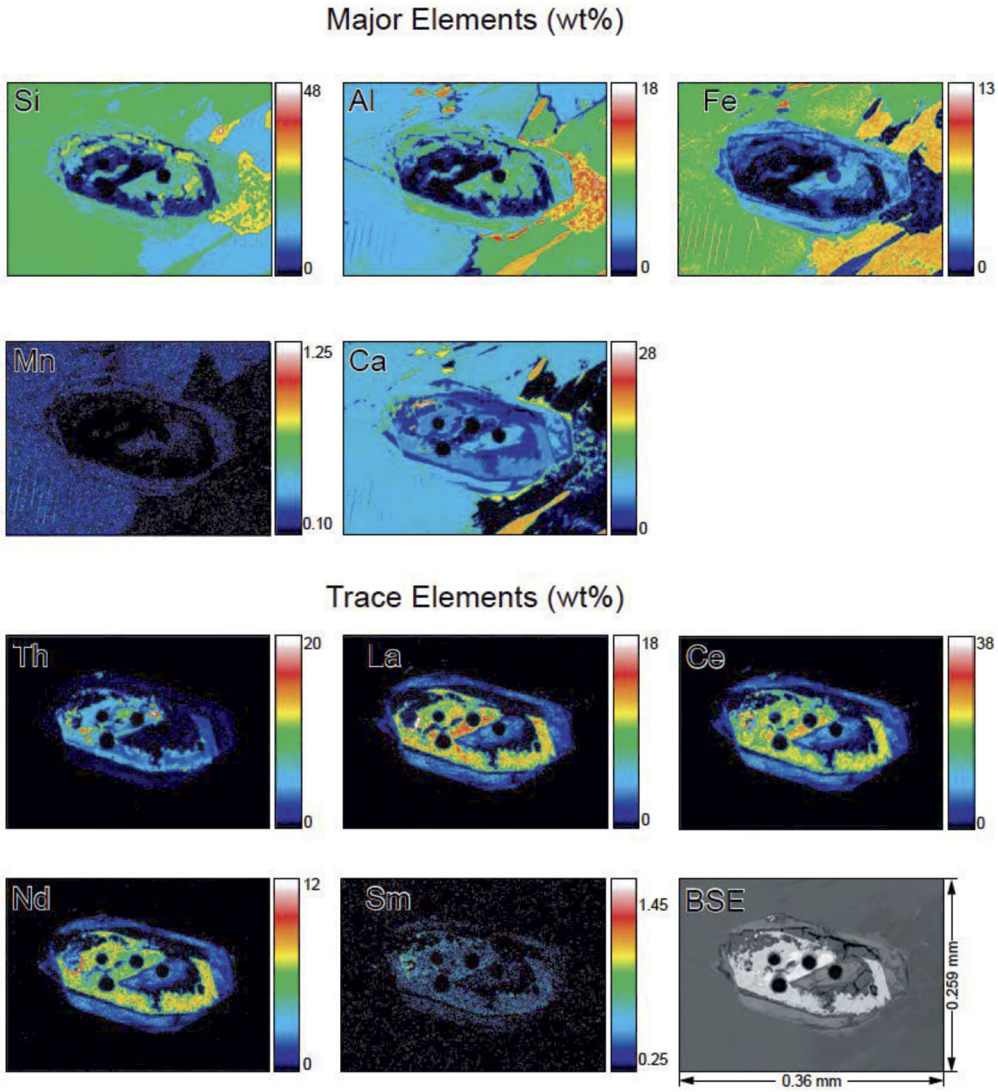


**Fig. 2.** Element distribution maps of a composite former allanite crystal (grain #3) in leucogabbro 15TKPB27 (in wt.%), showing the heterogeneity of element distribution between the secondary phases enriched in LREE. Bottom right panel shows BSE (Back-Scattered Electron images). EPMA point data and spot locations are shown in Appendix A-9.

*4.2.2. 18APPB20 leucogranitic gneiss*

Twenty-one analyses on nineteen different zircon grains were obtained. One analysis (18APPB20-12) returned a concordant $^{207}Pb/^{206}Pb$ date at $3.526 \pm 0.004$ Ga, suggesting ancient Pb loss and was discarded in further calculations. The remaining concordant analyses ($n = 9$) yield a cluster of $^{207}Pb/^{206}Pb$ dates that have a weighted mean of $3.576 \pm 0.004$ Ga (MSWD = 3.9; Fig. 4; Appendix Table A-3).

Eleven zircon O isotope analyses returned $\delta^{18}O$ values between 4.3 and 6.1‰, with a weighted mean of $5.3 \pm 0.4$‰ (MSWD = 1.3; Fig. 5; Appendix Table A-5). Thirteen analyses for Lu–Hf isotopes return $^{176}Hf/^{177}Hf$ ranging between 0.28052 and 0.28065, corresponding to $\varepsilon_{Hf(3.576\,Ga)}$ from −1.0 to +1.6 with a weighted mean of $-0.2 \pm 0.4$ (MSWD = 0.7) (Appendix Table A-6).

*4.2.3. 18APPB17 granodiorite*

Twenty analyses on eighteen different zircon grains yield twelve analyses that are discordant at the $2\sigma$ level. The remaining analyses cluster on concordia and give a weighted mean $^{207}Pb/^{206}Pb$ age of $3.433 \pm 0.004$ Ga (MSWD = 2.7; Fig. 4; Appendix Table A-3).

Twelve zircon O isotope analyses yield $\delta^{18}O$ values that range between 4.4 and 6.3‰, with a weighted mean of $5.4 \pm 0.3$‰ (MSWD = 0.7; Fig. 5; Appendix Table A-5). Fifteen Lu–Hf isotope analyses return $^{176}Hf/^{177}Hf$ ranging between 0.28057 and 0.28070, corresponding to $\varepsilon_{Hf(3.433\,Ga)}$ values from −0.8 to +0.5 with a weighted mean of $-0.4 \pm 0.2$ (MSWD = 0.8, Appendix Table A-6).

*4.3. U–Pb rutile data of gabbroic rocks*

Thirty-eight rutile grains (13 in 15TKPB25, 15 in 15TKPB26 and 10 in 15TKPB27) were analysed (Fig. 6 and Appendix Table A-4). As all three gabbros were sampled in proximity to each other and have 3.58 Ga zircon U–Pb ages, the rutile data are treated together. The measured U contents range from 4 to 103 ppm, and were mostly < 30 ppm. Common Pb, assessed by counts on mass 204, was negligible and no correction was applied. Analyses are less than 10% discordant at the $2\sigma$ level. The $^{207}Pb/^{206}Pb$ dates range from ca. 3.25 Ga to 2.84 Ga, with a majority of the data ($n = 22$) clustering between 2.98 and 2.94 Ga. One of these analyses (15TKPB25-9) was discarded due to a large uncertainty. The remaining analyses ($n = 21$) give a weighted mean $^{207}Pb/^{206}Pb$ age of $2.966 \pm 0.006$ Ga (MSWD = 2.4).

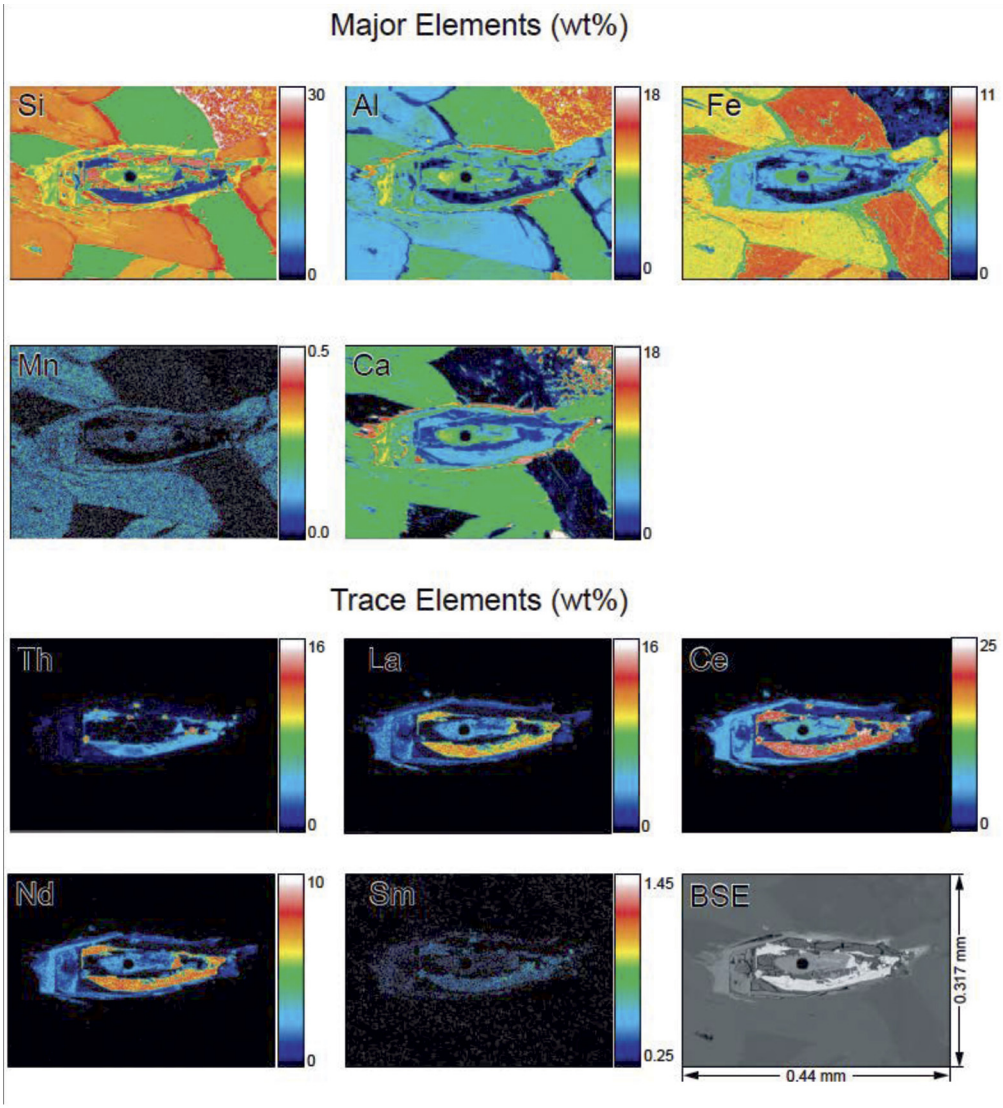


**Fig. 3.** Element distribution maps of a composition former allanite grain (grain #4) in 15TKPB27 (in wt.%), showing the heterogeneity of element distribution between the secondary phases enriched in LREE. The corresponding BSE image is shown in the bottom right panel, and EPMA point data and spot locations are shown in Appendix A-9.

### 4.4. Nd isotope data

#### 4.4.1. Whole-rock $^{147}Sm$–$^{143}Nd$ isotope data

The $^{143}Nd/^{144}Nd$ of the analysed rocks vary between 0.510602 ± 8 and 0.511174 ± 2, with a small spread of $^{147}Sm/^{144}Nd$ (0.109 to 0.133). Calculated at their respective U–Pb zircon crystallisation ages they return tightly clustered $\varepsilon_{Nd(3.580–3.575\ Ga)}$ between +0.1 and +0.9, with a weighted mean of +0.6 ± 0.3 (MSWD = 0.9) (Appendix Table A-2).

#### 4.4.2. Whole-rock $^{142}Nd$ isotopes

The $\mu^{142}Nd$ values of the gabbros and gneisses from Mount Webber range from −2.7 ± 1.5 to +2.8 ± 4.0 (2SE, ppm) (each sample was measured between one and four times; Appendix Table A-7). All these values are within the external reproducibility of the terrestrial Nd standard (JNdi-1), which gives an average $\mu^{142}Nd$ of 0 ± 5.4 ppm (2SD, $n = 6$). Hence, no resolvable $\mu^{142}Nd$ anomalies were detected in these, the oldest rocks of the Pilbara Craton.

#### 4.4.3. In-situ Nd isotope data on accessory minerals

Data from accessory minerals in all samples are listed in Appendix Table A-2, and plotted on Sm–Nd isochron diagrams in Fig. 7, together with the whole-rock analyses (plots for individual samples, with and without allanite are in Appendix A-11). We have not attempted to calculate an Sm–Nd budget based on these data, but note in the case of sample 15TKPB27 the position of the whole rock point relative to the mineral data requires the presence of an additional high Sm/Nd phase in the rock, which we suspect is hornblende (see Hammerli et al., 2019).

Collectively, the data form a scattered array on a Sm–Nd isochron diagram (Fig. 7a, Appendix Table A-2), with a nominal date of 3.098 ± 0.073 Ga (MSWD = 143) and an initial $^{143}Nd/^{144}Nd$ of 0.508502 ± 0.000075 ($\varepsilon_{Nd(3.098\ Ga)} = -2.4$). Analyses from the composite former allanite grains return by far the largest scatter (Fig. 7b), and tighter isochron regressions are generated if the allanite and apatite data are not considered. In sample 18APPB19 (dioritic gneiss), titanite and scheelite define an isochron date of 3.270 ± 0.032 Ga with an initial $^{143}Nd/^{144}Nd$ of 0.508178 ± 0.000055 ($2\sigma$, MSWD = 1.4, $\varepsilon_{Nd(i)} = -4.3$, Fig. 7c). Including the 18APPB19 whole-rock data-point gives a similar result, with an isochron date of 3.240 ± 0.018 Ga and an initial $^{143}Nd/^{144}Nd$ of 0.508237 ± 0.000023 ($2\sigma$, MSWD = 1.6, $\varepsilon_{Nd(i)} = -4.0$). These results are corroborated by an isochron generated using titanite analyses from 18APPB19 and 15TKPB24 (tonalitic gneiss), which spread over a considerable range of $^{147}Sm/^{144}Nd$ (0.15–0.36) and return a date of 3.234 ± 0.027 Ga with an initial $^{143}Nd/^{144}Nd$ of

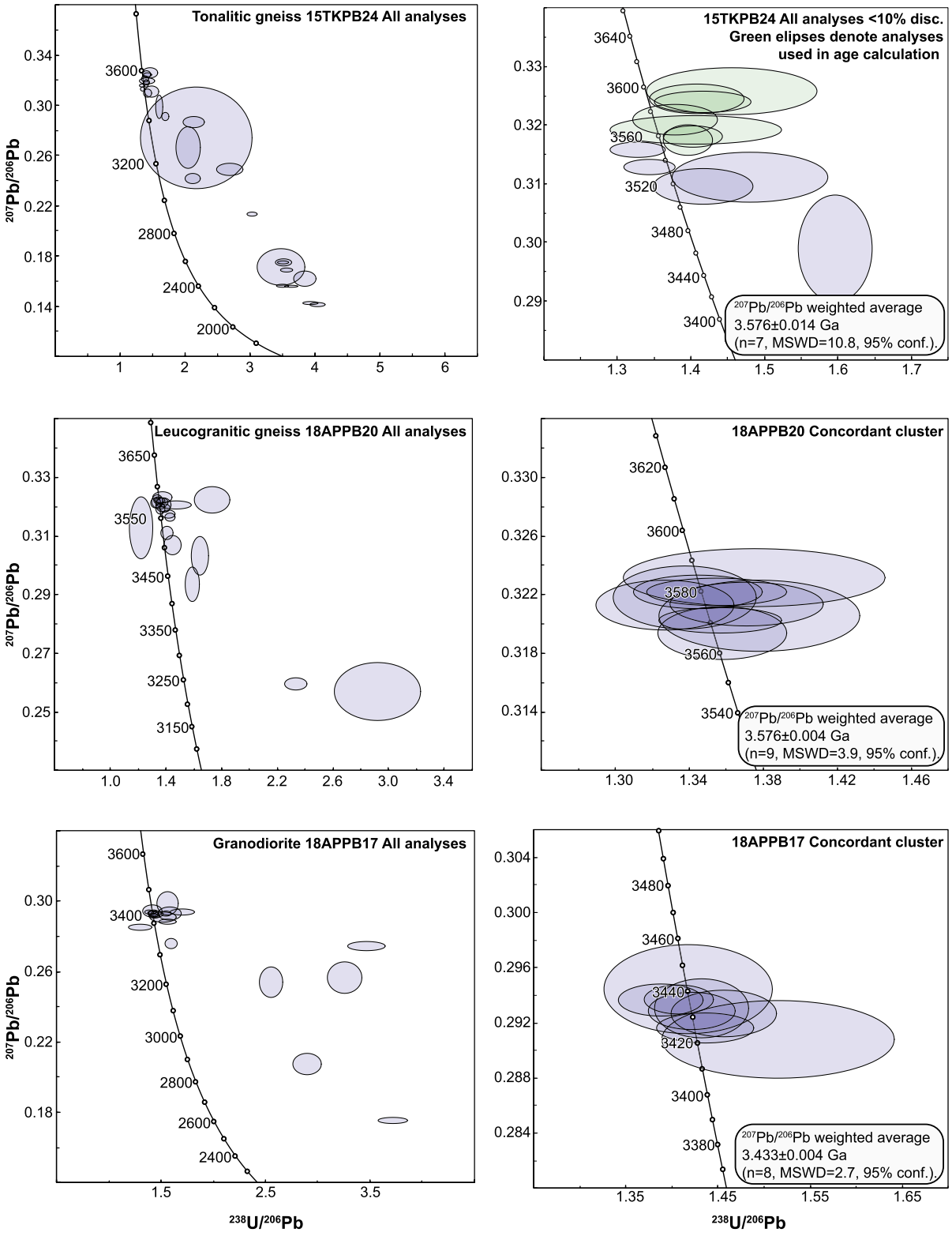


**Fig. 4.** Tera-Wasserburg diagrams showing SIMS (Secondary Ionisation Mass Spectrometry) zircon spot data for all samples ($2\sigma$ error ellipses). The left column shows all analyses and the right column shows data that were used in age calculations (if not otherwise noted). All data are reported in Appendix Table A-3.

$0.508256 \pm 0.000042$ ($2\sigma$, MSWD = 0.9, $\varepsilon_{Nd(i)} = -3.8$, Fig. 7d). The whole-rock data points from both of these samples plot on the regression lines defined by the mineral analyses on isochron diagrams.

Allanite data from individual samples show a large spread, with similar $^{143}Nd/^{144}Nd$ but highly variable $^{147}Sm/^{144}Nd$, from 0.03 to $\sim$ 0.15 (Fig. 7b). Within some grains, there is a correlation between BSE brightness and $^{147}Sm/^{144}Nd$, such that analyses located in the BSE bright domains return higher $^{147}Sm/^{144}Nd$, although the opposite pattern is shown by other grains; the highest $^{147}Sm/^{144}Nd$ (>0.07) are obtained from the BSE dark regions (REE-poor epidote; Appendix A-9). Time-resolved signals of indi-

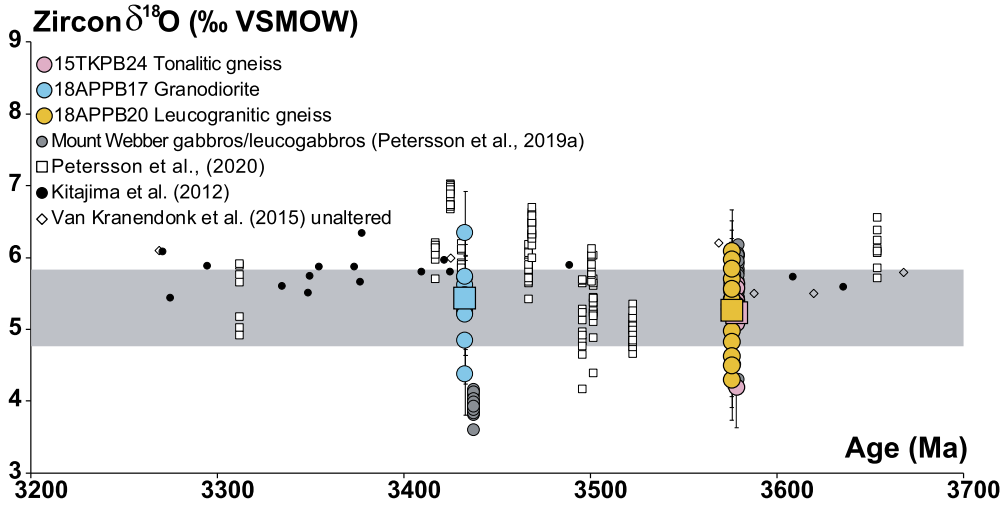


**Fig. 5.** Pilbara zircon $\delta^{18}O$ (‰, VSMOW) versus age (Ma) showing the consistently mantle like signatures of the Mount Webber rocks. All data can be found in Appendix Table A-5 (Petersson et al., 2019a, 2020; Kitajima et al., 2012; Van Kranendonk et al., 2015).

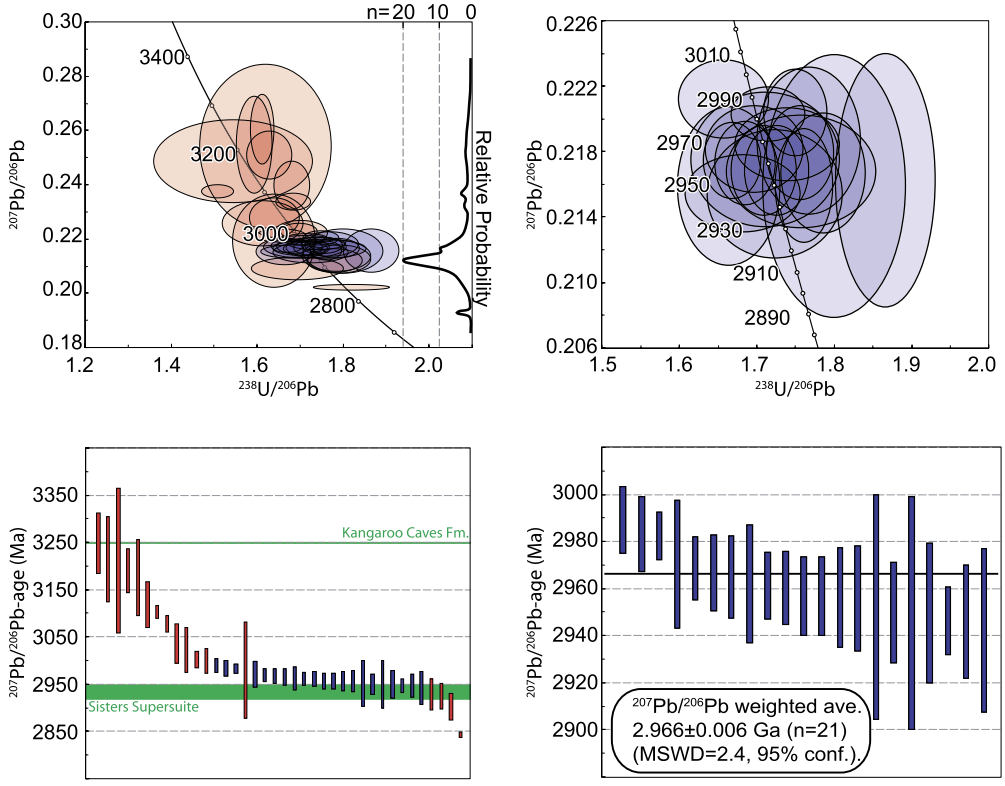


**Fig. 6.** Rutile U–Pb (SIMS) isotope data shown in Tera-Wasserburg and weighted average $^{207}Pb/^{206}Pb$ age plots. The left panels show all analysed data, and the right panels show the data used in age calculations. The blue shaded ellipses were used in age calculations, while the red shaded ellipses denote analyses not used in age calculations. All data are uncorrected for common Pb and are plotted at the $2\sigma$ level (see Appendix Table A-4).

vidual analyses are, however, complex, and show both increasing and decreasing $^{147}Sm/^{144}Nd$ with sampling depth, reflecting the mineralogical heterogeneity of the ablated volume (Appendix A-10). For this reason, correlating microstructural information from the polished grain surface with the down-hole Sm–Nd isotope data obtained by laser ablation analysis of these complex grains is difficult. In some cases, non-systematic time-resolved variations in $^{147}Sm/^{144}Nd$ are decoupled from variation in $^{143}Nd/^{144}Nd$ (e.g., 15TKPB27-1c), and one analysis (18APPB19-7b) shows down-hole increases in both $^{147}Sm/^{144}Nd$ and $^{143}Nd/^{144}Nd$ (see Appendix A-10).

## 5. Discussion

### 5.1. Refining the magmatic history of the Mount Webber type locality

Based on the zircon U–Pb data, samples 15TKPB24 (tonalitic gneiss) and 18APPB20 (leucogranitic gneiss) are interpreted to have protolith crystallisation ages of around 3.58 Ga (Fig. 4). These ages are consistent with the 3.59–3.58 Ga Mount Webber magmatic event, as defined by Petersson et al. (2019a) from gabbros and leucogabbros sampled from the same area. The age result from 18APPB20 is significant because it identifies silicic magmatism at

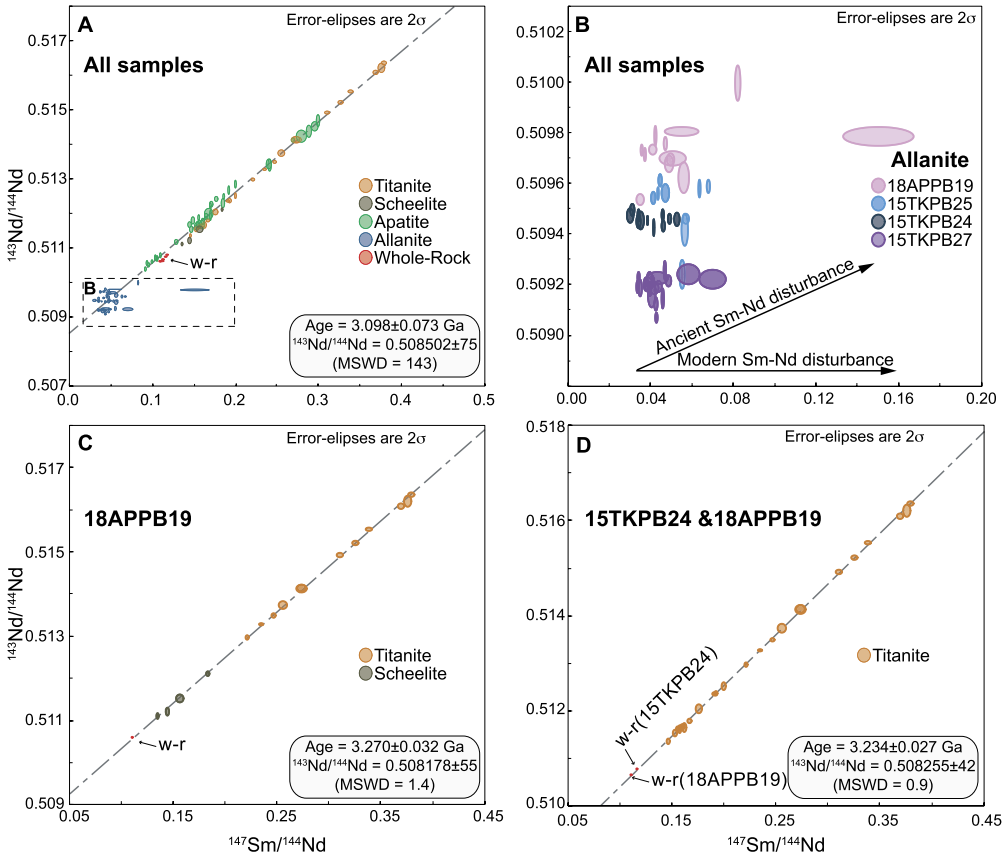


**Fig. 7.** Sm–Nd isochron diagrams plotting data from LA-ICP-MS analyses of allanite, titanite, apatite and scheelite, and whole-rock data from all analysed samples. A) An errorchron derived from all compiled data (Whole-rock ellipses have been increased slightly to aid visibility). B) Allanite data from individual samples showing trends that would result from recent versus ancient Sm–Nd disturbance. C) Isochron defined by titanite and scheelite from sample 18APPB19. D) Isochron derived from analyses of titanite from samples 15TKPB24 and 18APPB19.

Mount Webber to be coeval with the previously identified gabbroic component. This is in line with the tectonic model presented by Petersson et al. (2020), who envisage generation of the Mount Webber gabbros by decompression melting of the mantle during incipient rifting of a thickened proto-crust at ca. 3.59 Ga, where melting of juvenile mafic crust at depth also generated the oldest granitic magmas. Granodiorite 18APPB17 is interpreted to have crystallised at 3.433 ± 0.004 Ga, coeval with the 15TKPB23 gabbro identified by Petersson et al. (2019a) and correlating with the Tambina granitic suite that comprises a major part of the Shaw Granitic Complex. This indicates that the second episode of magmatism in the Mount Webber area also included emplacement of both mafic and granitic rocks.

### *5.2. Timing of post-magmatic thermal events and their geological significance*

The well-defined Nd isochrons from titanite (in sample 15TKPB24 and 18APPB19) and scheelite (in 18APPB19) (Fig. 7c–d, Appendix Table A-2) suggest that the Sm–Nd system was equilibrated on a mineral scale at ca. 3.25 Ga. Considering the occurrence of the hydrothermal mineral scheelite ($CaWO_4$) in the diorite 18APPB19, fluid ingress (which mobilised W and the REE) is the most likely cause of isotope homogenisation at this time. Furthermore, the textural occurrence of titanite grains in these samples (haloes around ilmenite; Petersson et al., 2019a, Appendix A-8) is consistent with formation during a metamorphic event. The closest dated 3.25 Ga igneous rock is a metamorphosed rhyolite (3.245 ± 0.002 Ga) at Black Hill Well, 40 km to the WNW. However, volcanic and sedimentary rocks correlated with the ca. 3.25 Ga Kangaroo Caves Formation crop out approximately 3 kilometres to the west and to the east of the sample locality (Fig. 1). As these rocks host microfossils (Rasmussen, 2000) and organic carbon (Rasmussen and Buick, 2000), hydrothermal fluid circulation has been suggested to accompany the deposition of this formation in a hot spring environment. The 3.27–3.23 Ga Sm–Nd isochron dates from Mount Webber are therefore interpreted to be geologically significant, and to reflect the distal effects of hydrothermal activity related to deposition of the Kangaroo Caves Formation.

Rutile U–Pb analyses yield a 2.966 ± 0.006 Ga age that is previously unknown to the Mount Webber area (Fig. 6). Given that the rutile petrographically appears to be a primary igneous phase that crystallised at 3.59 Ga (Petersson et al., 2019a), the U–Pb result is interpreted to represent partial to complete Pb-loss in rutile during a younger thermal event. One possibility is that this was related to activity on the Mulgandinnah Shear Zone, for which a minimum age of 2.944 ± 0.009 Ga was determined by Ar–Ar on hornblende from a locality ten kilometres east of the Mount Webber gabbros (Zegers et al., 1999). Alternatively, U–Pb resetting of rutile may have been related to emplacement of the 2.95–2.92 Ga Sisters Supersuite, several granitic intrusions of which crop out within 10–20 kilometres of the Mount Webber locality. The rutile U–Pb age at Mount Webber is, however, 35 million years older than the crystallisation age of these granites, which clusters around 2.93 Ga (see Appendix A-4 for details). The rutile data could register a slightly earlier thermal event preceding intrusion of the Sisters Supersuite in the Mount Webber area, as is also suggested in the Ar–Ar data of Zegers et al. (1999), or reflect minor retention of older radio-

genic Pb in the rutile grains. The latter interpretation agrees with the scattering of $^{207}Pb/^{206}Pb$ dates that are older than 3 Ga (Fig. 6).

### 5.3. Cause of disturbed of allanite Sm–Nd isotope systematics

A prominent feature of the in-situ Nd isotope dataset is that analyses from the composite allanite grains do not conform to the isochronous relationships defined by apatite and titanite in the Mount Webber samples. The implication is that allanite behaved differently to the other REE-bearing accessory minerals in these rocks. The decay of U and Th dislocates the crystal structure of minerals making ancient high U and Th minerals like allanite especially prone to alteration and physiochemical weathering (Morin, 1977). During weathering and oxidation, structurally-compromised allanite breaks down to form secondary monazite ($(Ce,La,Nd,Th)PO_4$), and numerous other phases, including cerianite ($(Ce,Th)O_2$) and lanthanite ($(REE)_2(CO_3)_3{\cdot}8(H_2O)$). These mineral phases are the major sinks of REE and Th produced during allanite alteration (Meintzer and Mitchell, 1988). In a tonalitic gneiss, two-thirds of the Nd and one third of the Sm may be contained in allanite (Hammerli et al., 2019). As allanite hosts such a dominant portion of the Sm and Nd budget in tonalitic gneisses, allanite break-down could potentially lead to disturbance of the Sm–Nd system, at least on a local scale (Hammerli et al., 2019; Wang et al., 2022).

In the present study, the whole-rock data points plot close to the composite former allanite analyses (Fig. 7a), suggesting that allanite was also the dominant carrier of LREE in the Mount Webber samples. Furthermore, as illustrated in Fig. 7b, analyses of the 'allanite' grains in all samples have fairly homogeneous $^{143}Nd/^{144}Nd$, but variable $^{147}Sm/^{144}Nd$. The horizontal spread of the allanite analyses on an Sm–Nd isochron diagram suggests recent disturbance, as ancient resetting would generate a non-horizontal array, the slope of which depends on the age of the disturbance event. This pattern does not, however, preclude earlier events to have affected the allanite, as the isotopic data would register the latest disturbance.

We interpret the disturbance of allanite Sm–Nd systematics to reflect break down of these mineral grains during modern weathering. As noted above, individual former allanite grains now comprise a complex, heterogeneous mixture of material with different compositions, including REE-phosphate, epidote (REE-rich and REE-poor) and spongy-textured material that may be REE-carbonate. We infer that this assemblage is the result of extensive interaction between metamict magmatic allanite and percolating fluids, which variably mobilised and redistributed Ca and the REE. The horizontal $^{147}Sm/^{144}Nd$ scatter on Fig. 7b is therefore attributed to incorporation into the laser ablation analysis of secondary, recrystallised REE-rich material that formed recently. This effect is evident in individual analyses (see Appendix A-10, C-D) The down-hole increase in both $^{147}Sm/^{144}Nd$ and $^{143}Nd/^{144}Nd$ shown by one analysis (Appendix A-10) is interpreted to reflect radiogenic ingrowth, indicating that the variable $^{147}Sm/^{144}Nd$ of that analysed volume must have developed at some time in the past. This could suggest that the allanite grains in these samples record several events of Sm–Nd disturbance.

The behaviour of allanite has implications for other isotopic methods used to trace ancient crust-mantle differentiation. The $^{138}La–^{138}Ce$ isotope system has recently been used in studies of planetary evolution (e.g., Israel et al., 2020), including in the Pilbara Craton (Hasenstab et al., 2021), and in felsic rocks the parent and daughter elements will be concentrated in accessory minerals such as monazite and allanite. Hasenstab et al. (2021) report a narrow range of near-chondritic initial Ce isotope compositions for mafic rocks of the Pilbara Craton, but a 'surprising' scatter in $Ce/Ce^*$ and $\varepsilon_{Ce(i)}$ values for the granitic rocks. The variation in latter is attributed to the felsic rocks being more susceptible to weathering than the mafic samples, despite the 'seemingly pristine mineralogy and....very low LOIs ($<1.5\%$)'. We suggest that the disturbance of the $^{138}La–^{138}Ce$ isotope system in the silicic rocks potentially relates to the alteration of metamict allanite (or monazite) in those samples. Petrographic examination of samples in our collection from two of the granitic units targeted by Hasenstab et al. (2021) (North Shaw Tonalite and Spear Hill Monzogranite) confirms the presence of metamict allanite. The possibility that allanite alteration imparts secondary variation in $\varepsilon_{Ce(i)}$, as it can for $\varepsilon_{Nd(i)}$ (Hammerli et al., 2019), underlines the importance of detailed petrography to assess the state of preservation of the main mineralogical hosts of the isotope tracer systems being considered for whole rock studies.

### 5.4. Whole-rock Sm–Nd response to Nd mobility in minerals

The errorchron date of $3.098 \pm 0.073$ Ga yielded by the in situ and whole rock Sm–Nd isotope data is substantially younger than the protolith crystallisation ages of the Mount Webber samples ($\sim$3.58 Ga), as determined by zircon U–Pb data. Sm–Nd data from individual samples (whole-rock + minerals) also scatters considerably, with errorchon dates ranging between 3.50 Ga and 2.85 Ga, all with MSWD $\geq$54 (Appendix A-11). This disparity between the Sm–Nd errorchron dates and the zircon U–Pb crystallisation ages, together with the complex Sm–Nd systematics of the major mineral host (allanite) of Sm and Nd, suggests post-magmatic re-homogenisation of the Sm–Nd systematics of the Mount Webber rocks. A pertinent question concerns whether this post-magmatic Sm–Nd disturbance was open versus closed system at the scale of sampling, since this determines whether initial $^{143}Nd/^{144}Nd$ ratios determined from whole rock Sm–Nd data are reliable. Hammerli et al. (2019) and Wang et al. (2022) both argue that Sm–Nd mobility during allanite decomposition can generate geologically meaningless initial whole-rock Nd isotope signatures with spurious positive or negative $\varepsilon_{Nd}$ values.

Fig. 8 plots the Nd isotope composition calculated back in time of the individual minerals and whole-rock samples from the analysed Mount Webber samples. Titanite, and to some extent, scheelite have evolutionary arrays that converge at ca. 3.25 Ga, indicating Sm–Nd homogenisation at this time, whereas analyses from apatite and the composite allanite grains define complex arrays with no unique convergence point. Importantly, despite the Sm–Nd complexity of the constituent minerals, the evolutionary trajectories of the whole-rock analyses converge to the most minimal spread of initial Nd isotope ratios at the time of igneous crystallisation determined by zircon U–Pb isotopes (Fig. 8). This observation advocates for Sm–Nd isotopic integrity of the whole rock system, and suggests that the average whole rock $\varepsilon_{Nd}$ value of +0.6 has geological significance. A further observation in support of this is that the whole rock Nd – zircon Hf isotope signatures are coupled and plot within the 'Terrestrial Array' of Vervoort et al. (2011), overlapping with data from other well preserved Pilbara Craton igneous samples (Fig. 9; see below). Minor open system behaviour associated with metamorphism and alteration of allanite in the Mount Webber rocks cannot be precluded – however, given the tight clustering of $\varepsilon_{Nd(3.58\ Ga)}$ values, and that the well-defined mineral Sm–Nd isochrons of several samples also include the whole-rock data point, mobility of the REE at the whole rock scale appears have been limited.

The reason why the Sm–Nd system in the Mount Webber rocks remained intact at a whole-rock scale, in contrast to the rocks studied by Hammerli et al. (2019) and Wang et al. (2022), may be due to the degree of metamorphism and the temperature of allanite decomposition. Hammerli et al. (2019) studied Eoarchean tonalitic gneisses from Greenland that were overprinted

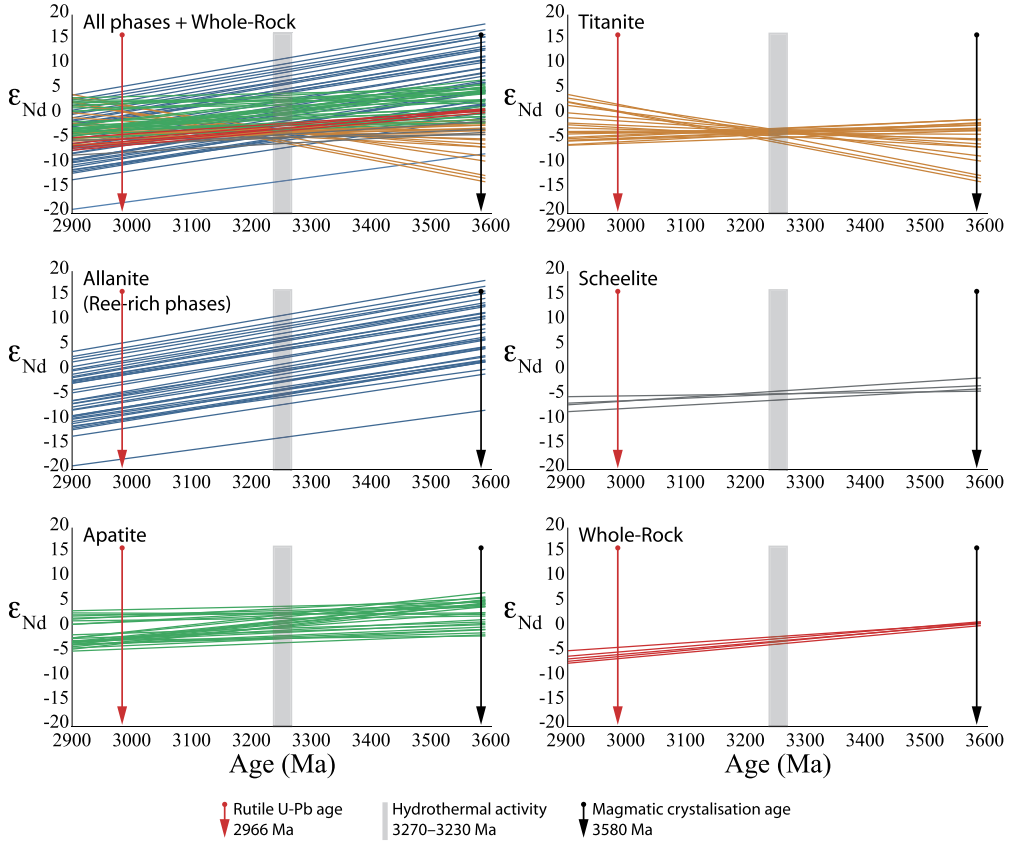


**Fig. 8.** $^{143}Nd/^{144}Nd$ and $\varepsilon_{Nd(t)}$ versus time for individual minerals and the whole-rock analyses. Evolutionary arrays that converge after the time of igneous crystallisation indicate resetting of the Sm/Nd isotope system at the time of intersection. Whole-rock data arrays converge to a point in line with the age of igneous crystallisation, suggesting minimally-disturbed isotopic information at the sampled scale.

by regional granulite facies metamorphism in the Neoarchean, and Wang et al. (2022) studied gneisses from the Minnesota River Valley that record peak metamorphic conditions of 0.45–0.75 GPa and 650–750 °C, hence upper amphibolite to granulite facies (Moecher et al., 1986). Both studies demonstrate disturbance of the whole-rock system, caused by the element mobility from REE-rich minerals, and associated variability in whole rock $\varepsilon_{Nd}$ values. The Mount Webber gabbros are pervasively metamorphosed, and although quantitative P-T estimates are not available, these samples contain deformational fabrics defined by blue-green hornblende and biotite (i.e., amphibolite facies, Petersson et al., 2019a). Coupled whole-rock Hf–Nd isotope systematics are also reported for Pilbara Craton igneous rocks by Salerno et al. (2021), these being weakly deformed granitic rocks metamorphosed in the greenschist facies. At Mount Webber, we infer that breakdown of metamict allanite occurred during near-surface weathering, such that the REE released by this process were sequestered by low temperature secondary minerals, rather than being fugitive in metamorphic fluids at higher temperatures. This contributed to preservation of the original magmatic Nd isotope signatures in these gneisses.

### 5.5. Implications for crustal evolution studies

Several studies have observed that zircon Hf isotope signatures of Eo- and Paleoarchaean meta-igneous rocks are dominantly chondritic to mildy superchondritic (Kemp and Hawkesworth, 2014; Fisher and Vervoort, 2018; Petersson et al., 2020; Fig. 9a). This includes samples from the Pilbara Craton (Petersson et al., 2019a, 2020; Murphy et al., 2021; Salerno et al., 2021; Kemp et al., 2023), including the Mount Webber Gabbros, as previously reported by Petersson et al. (2019a). With zircon $\varepsilon_{Hf}$ values near zero, data from the present study align with this outcome. The consistent mantle-like $\delta^{18}O$ values agree with previously published data from the Mount Webber leucogabbros (Petersson et al., 2019a, 2020), and signal minimal input from $^{18}O$-enriched (or $^{18}O$-depleted) supracrustal material into the Mount Webber samples. Taken together, the zircon O–Hf data are interpreted to indicate derivation of the parent magmas from an approximately undifferentiated mantle source (Fig. 10, see also Petersson et al., 2019a, 2019b, 2020). This conclusion receives support from the whole rock $\varepsilon_{Nd(3.58\ Ga)}$ values of the Mount Webber rocks, which range from +0.1 to +0.9.

Recent papers by Frossard et al. (2022) and Johnston et al. (2022) show that the Earth's mantle has a small $^{142}Nd$ excess of ca. 8–10 ppm relative to an undifferentiated body coming from the non-carbonaceous reservoir. To produce this radiogenic excess in $^{142}Nd$, the Sm/Nd must be slightly super-chondritic, and Frossard et al. (2022) propose a Bulk Silicate Earth (BSE) $^{147}Sm/^{144}Nd$ of 0.2012, with fractionation at the beginning of solar system formation due to the loss of primordial crusts in planetesimals by collisional erosion. As seen in Fig. 9C, the Nd isotope data from our Mount Webber samples fall on this line.

As noted above, the whole-rock Nd isotope signatures of felsic Paleoarchean rocks from the Pilbara Craton scatter over nearly 4 epsilon units (−2 to +2, Fig. 9c). The cause of this dispersion is yet to be determined – one possibility is that it reflects heterogeneous magma sources due to mixing between depleted mantle-like and ancient crustal components (e.g., Gardiner et al., 2017). Some studies report more consistent results, however. Salerno et al. (2021) determine whole rock $\varepsilon_{Nd(3.47–3.28\ Ga)}$ values clustering just above chondritic (+0.1 to +1.2) for six TTGs from the Mount Edgar Granitic Complex. For these samples, the veracity of the whole

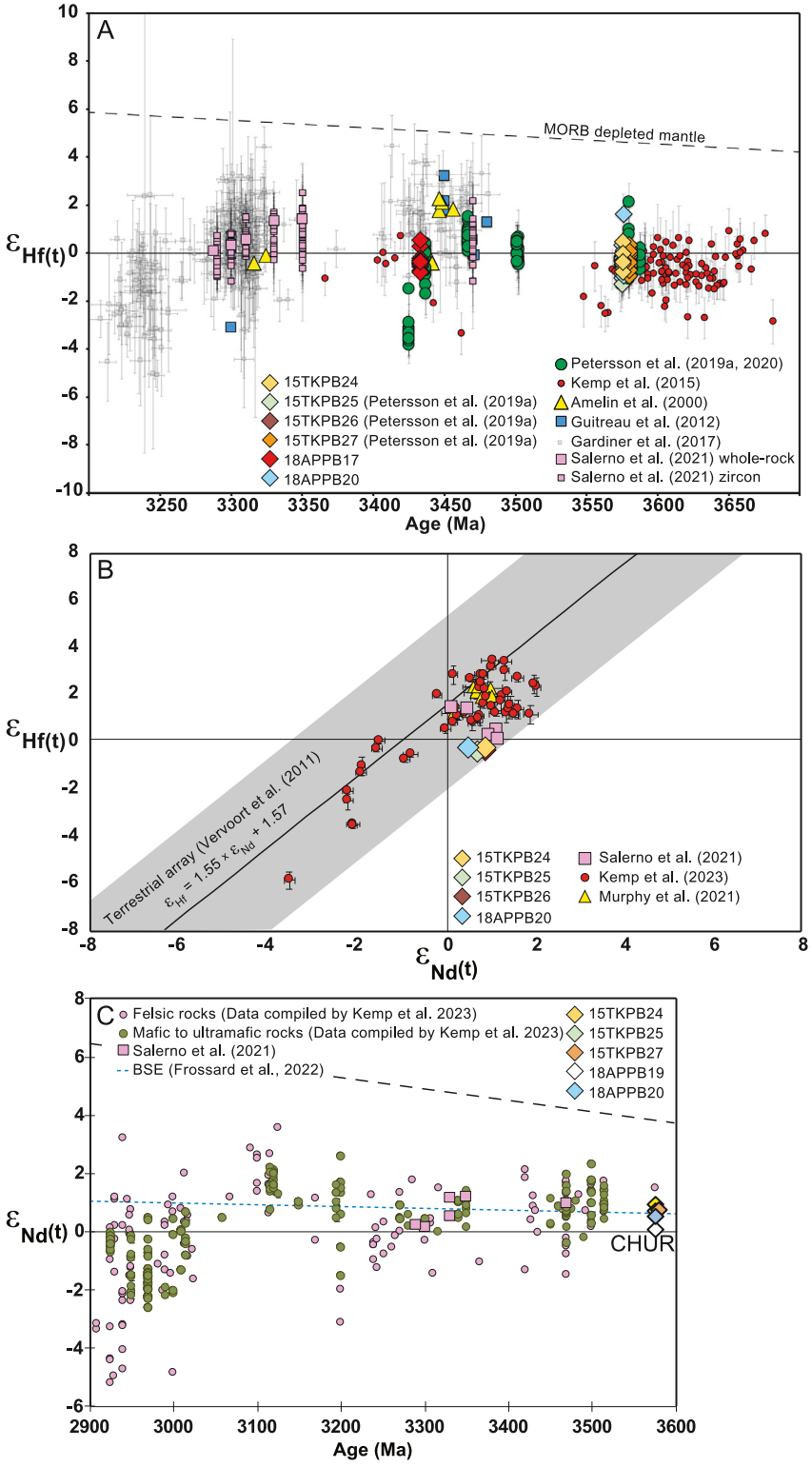


**Fig. 9.** A) Zircon $\varepsilon_{Hf}$ versus crystallisation age (in Ma) highlighting the dominantly chondritic Hf isotope signatures of zircon grains from the Eo- and Paleoarchean Pilbara Craton. All data are from the East Pilbara Terrane (Petersson et al., 2019a, 2020; Kemp et al., 2015; Amelin et al., 2000; Guitreau et al., 2012; Gardiner et al., 2017; Salerno et al., 2021). B) Initial $\varepsilon_{Nd}$ vs. $\varepsilon_{Hf}$ for the samples included in this study, granitic rocks from Salerno et al. (2021), and mafic and ultramafic rocks from Murphy et al. (2021) and Kemp et al. (2023). All samples are from the East Pilbara Terrane and fall within the envelope defined by initial isotope values from global compilations of igneous rocks ($\varepsilon_{Hf} = 1.5 \times \varepsilon_{Nd} + 1.57$; Vervoort et al., 2011). C) Whole rock Nd isotope composition of igneous rocks from the Pilbara Craton. The bulk silicate Earth (BSE) evolution proposed by Frossard et al. (2022) is shown as a blue dashed line.

rock Nd data is supported by some constituent LREE-rich minerals (apatite and titanite) yielding Sm–Nd isochron dates that are the same as the magmatic emplacement ages determined by zircon U–Pb. Whole-rock Nd isotopes from texturally well-preserved granites, granodiorites and tonalites from the North Shaw Suite (McCulloch, 1987; Bickle et al., 1993) yield $\varepsilon_{Nd(3.49–3.47\ Ga)}$ of +1.3 to −1.3, giving a weighted average of $0.4 \pm 0.5$ (2SD, $n = 6$), also within uncertainty of the chondritic reference. Alternatively, the

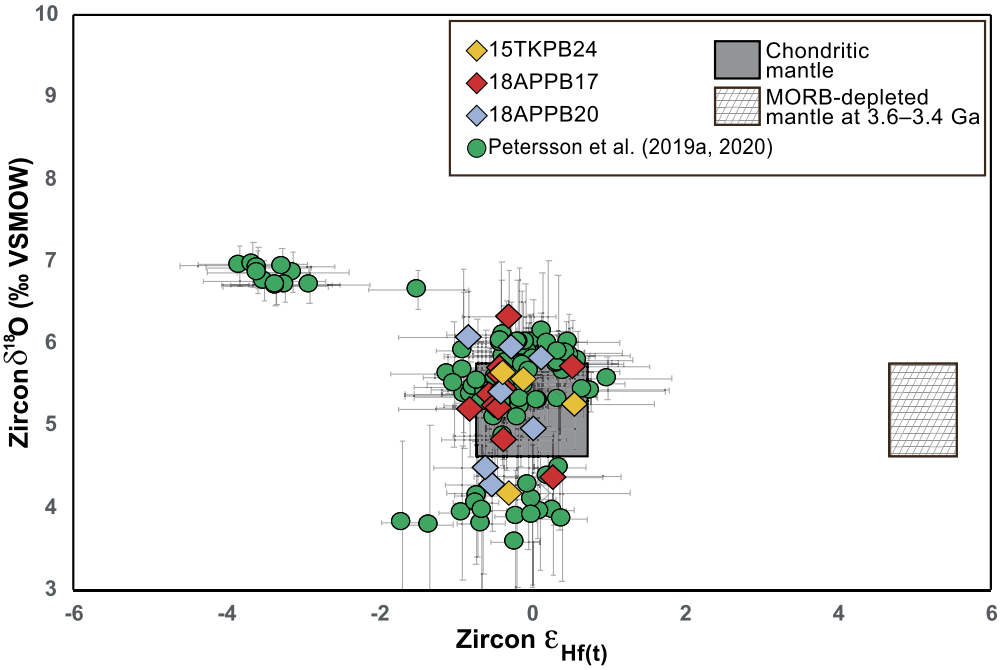


**Fig. 10.** A plot of zircon $\varepsilon_{Hf}$ versus $\delta^{18}O$, showing overwhelmingly mantle-like O isotope and chondritic Hf isotope signatures, suggesting a chondritic mantle composition at the time of zircon crystallisation. Grey box denotes the field that represents a chondritic mantle composition and is defined by the zircon $\delta^{18}O = 5.3 \pm 0.6‰$ mantle value of Valley et al. (2005) and the $\varepsilon_{Hf} = 0 \pm 0.4$ CHUR value of Bouvier et al. (2008). The checkered box denotes a field that represent a model MORB-source depleted mantle composition at 3.6–3.4 Ga.

whole rock Nd isotope scatter of the Paleoarchean Pilbara granites could reflect the multi-component nature of some of the analysed banded gneisses, or Sm–Nd isotope disturbance during metamorphism and deformation – both of these possibilities can be tested by microanalysis of LREE-rich minerals, as advocated here.

There has been debate about the extent to which the preserved Paleoarchean eruptive sequences of the Pilbara Craton accumulated on an older (Eoarchean) continental substrate (see Kemp et al., 2023). The near-chondritic whole-rock $^{143}Nd/^{144}Nd$ and zircon $^{176}Hf/^{177}Hf$ signatures for the 3.59–3.58 Ga meta-igneous rocks from the Mount Webber area provide no evidence for sampling of $>$ 3.7 Ga continental crust beneath the Pilbara Craton. The lack of resolvable $^{142}Nd$ anomalies in the Mount Webber rocks further negates any contribution from a Hadean source component with fractionated Sm/Nd. This finding accords with previous $^{142}Nd$ studies from mafic rocks of the Pilbara Craton (Archer et al., 2019; Murphy et al., 2021) that did not detect $^{142}Nd$ anomalies.

## 6. Conclusions

Whether the complex whole rock Sm–Nd record of ancient terrestrial samples reflects early differentiation of silicate Earth reservoirs or is an artefact of metamorphic disturbance remains contentious. Here, we employ a combined *in situ* and whole-rock analytical approach to show that despite multiple metamorphic episodes and breakdown of the mineral that controls the REE budget of these rocks (i.e., allanite), the 3.59–3.58 Ga gneisses at Mount Webber retain their Sm–Nd isotope integrity at the whole-rock scale and preserve the signatures of the original magmatic protoliths. We attribute this to approximately closed system behaviour during disturbance of mineral Sm–Nd systematics, reflecting the decomposition of allanite at low temperatures during near-surface oxidative weathering. Under these conditions, the LREE were redistributed into an assemblage of secondary minerals with variable Sm/Nd, rather than partitioning into higher temperature metamorphic fluids moving through the rocks.

We show that valuable information about the thermal evolution of ancient terranes can be retrieved by *in situ* isotope analyses of accessory minerals, particularly those with variable Sm/Nd. In this study, the Sm–Nd isotope analyses of titanite, apatite, allanite and scheelite, in combination with rutile and zircon U–Pb data, reveal a complex thermal history at Mount Webber, with isotopic disturbances recorded at ~3.25 Ga and 2.96 Ga. These are interpreted to record hydrothermal activity associated with emplacement of the 3.25 Ga Kangarroo Caves Formation and a metamorphic event that may have been related to intrusion of the 2.95–2.92 Ga Sisters Supersuite.

Microanalysis of REE-rich accessory minerals is a powerful tool for assessing the reliability of the whole rock Sm–Nd isotope systematics of ancient felsic rocks (Hammerli et al., 2019; Salerno et al., 2021), and whether these convey geologically meaningful petrogenetic information. The 3.59–3.58 Ga Mount Webber rocks exhibit no signs of Nd–Hf isotope decoupling, and exhibit whole-rock Sm–$^{142,143}Nd$ and zircon Lu–Hf and O isotope signatures that are compatible with the parent mafic and felsic magmas representing juvenile additions to the Pilbara Craton. These rocks were derived from a mantle source that preserves no evidence for silicate Earth differentiation in the Hadean.

## CRediT authorship contribution statement

**Andreas Petersson:** Conceptualization, Funding acquisition, Investigation, Writing – original draft, Writing – review & editing. **Anthony I.S. Kemp:** Conceptualization, Funding acquisition, Investigation, Supervision, Writing – review & editing. **Maud Boyet:** Investigation, Writing – review & editing. **Martin J. Whitehouse:** Investigation, Resources, Writing – review & editing. **Matilda Boyce:** Investigation, Writing – review & editing. **Malcolm Roberts:** Investigation, Writing – review & editing. **Allen Kennedy:** Investigation, Writing – review & editing.

## Declaration of competing interest

The authors declare that they have no known competing financial interests or personal relationships that could have appeared to influence the work reported in this paper.

## Data availability

All data provided as supplemental files.

## Acknowledgements

Financial support to A. Petersson by the Swedish Research Council (grant VR#2016-00261) and from the Danish Independent Research Fund (grant: 9040-0374B) is gratefully acknowledged. AK acknowledges an Australian Research Council Future Fellowship (FT10010059) and field logistic support from the Geological Survey of Western Australia. MB received funding from the European Research Council (ERC) under the European Union's Horizon 2020 research and innovation program (grant agreement no. 6822778). Nd and Hf isotope analyses at UWA were conducted with instrumentation funded by the Australian Research Council (LE100100203 and LE150100013). The authors acknowledge the facilities and the scientific and technical assistance of the Centre of Microscopy, Characterisation and Analysis (CMCA), The University of Western Australia, a facility funded by the University, State and Commonwealth Governments. The NordSIMS ion microprobe facility operates as Swedish-Icelandic infrastructure, partly funded by the Swedish Research Council (grant no. 2017-00671). The authors acknowledge Marion DeFrance who participated in the project during her Master's degree. This is Nordsim contribution #736.

## Appendix A. Supplementary material

Supplementary material related to this article can be found online at https://doi.org/10.1016/j.epsl.2023.118346.

## References

Allègre, C.J., Rousseau, D., 1984. The growth of the continent through geological time studied by Nd isotope analysis of shales. Earth Planet. Sci. Lett. 67 (1), 19–34.
Amelin, Y., Lee, D.C., Halliday, A.N., 2000. Early-middle Archaean crustal evolution deduced from Lu-Hf and U-Pb isotopic studies of single zircon grains. Geochim. Cosmochim. Acta 64 (24), 4205–4225.
Archer, G.J., Brennecka, G.A., Gleißner, P., Stracke, A., Becker, H., Kleine, T., 2019. Lack of late-accreted material as the origin of 182W excesses in the Archean mantle: evidence from the Pilbara craton, western Australia. Earth Planet. Sci. Lett. 528, 115841.
Bauer, A.M., Fisher, C.M., Vervoort, J.D., Bowring, S.A., 2017. Coupled zircon Lu–Hf and U–Pb isotopic analyses of the oldest terrestrial crust, the > 4.03 Ga Acasta Gneiss complex. Earth Planet. Sci. Lett. 458, 37–48.
Bennett, V.C., 2003. Compositional evolution of the mantle. In: Carlson, R.L. (Ed.), Treatise on Geochemistry. Elsevier, pp. 493–519.
Bickle, M.J., Bettenay, L.F., Barley, M.E., Chapman, H.J., Groves, D.I., Campbell, I.H., De Laeter, J.R., 1983. A 3500 Ma plutonic and volcanic calc-alkaline province in the Archaean East Pilbara Block. Contrib. Mineral. Petrol. 84, 25–35.
Bickle, M.J., Bettenay, L.F., Chapman, H.J., Groves, D.I., McNaughton, N.J., Campbell, I.H., de Laeter, J.R., 1993. Origin of the 3500–3300 Ma calc–alkaline rocks in the Pilbara Archean: isotopic and geochemical constraints from the Shaw Batholith. Precambrian Res. 60, 117–149.
Bouvier, A., Vervoort, J.D., Patchett, P.J., 2008. The Lu–Hf and Sm–Nd isotopic composition of CHUR: constraints from unequilibrated chondrites and implications for the bulk composition of terrestrial planets. Earth Planet. Sci. Lett. 273, 48–57.
Bowring, S.A., Housh, T., 1995. The Earth's early evolution. Science 269 (5230), 1535–1540.
Carlson, R.W., Garçon, M., O'Neil, J., Reimink, J., Rizo, H., 2019. The nature of Earth's first crust. Chem. Geol. 530, 119321.
DePaolo, D.J., Linn, A.M., Schubert, G., 1991. The continental crustal age distribution; methods of determining mantle separation ages from Sm–Nd isotopic data and application to the southwestern United States. J. Geophys. Res. 96, 2071–2088.
Fisher, C.M., Vervoort, J.D., 2018. Using the magmatic record to constrain the growth of continental crust—the Eoarchean zircon Hf record of Greenland. Earth Planet. Sci. Lett. 488, 79–91.
Fisher, C.M., Bauer, A.M., Vervoort, J.D., 2020. Disturbances in the Sm–Nd isotope system of the Acasta Gneiss Complex—Implications for the Nd isotope record of the early Earth. Earth Planet. Sci. Lett., 115900.
Frossard, P., Israel, C., Bouvier, A., Boyet, M., 2022. Earth's composition was modified by collisional erosion. Science 377 (6614), 1529–1532.
Gardiner, N.J., Hickman, A.H., Kirkland, C.L., Lu, Y., Johnson, T., Zhao, J.X., 2017. Processes of crust formation in the early Earth imaged through Hf isotopes from the East Pilbara Terrane. Precambrian Res. 297, 56–76.
Guitreau, M., Blichert-Toft, J., Martin, H., Mojzsis, S.J., Albarède, F., 2012. Hafnium isotope evidence from Archean granitic rocks for deep-mantle origin of continental crust. Earth Planet. Sci. Lett. 337, 211–223.
Guitreau, M., Boyet, M., Paquette, J.L., Gannoun, A., Konc, Z., Benbakkar, M., Suchorski, K., Hénot, J.M., 2019. Hadean protocrust reworking at the origin of the Archean Napier Complex (Antarctica). Geochem. Perspect. Lett. 12, 7–11.
Hammerli, J., Kemp, A.I., Whitehouse, M.J., 2019. In situ trace element and Sm-Nd isotope analysis of accessory minerals in an Eoarchean tonalitic gneiss from Greenland: implications for Hf and Nd isotope decoupling in Earth's ancient rocks. Chem. Geol. 524, 394–405.
Hasenstab, E., Tusch, J., Schnabel, C., Marien, C.S., Van Kranendonk, M.J., Smithies, H., Howard, H., Maier, W.D., Münker, C., 2021. Evolution of the early to late Archean mantle from Hf-Nd-Ce isotope systematics in basalts and komatiites from the Pilbara Craton. Earth Planet. Sci. Lett. 553, 116627.
Hoffmann, J.E., Münker, C., Polat, A., Rosing, M.T., Schulz, T., 2011. The origin of decoupled Hf–Nd isotope compositions in Eoarchean rocks from southern West Greenland. Geochim. Cosmochim. Acta 75 (21), 6610–6628.
Israel, C., Boyet, M., Doucelance, R., Bonnand, P., Frossard, P., Auclair, D., Bouvier, A., 2020. Formation of the Ce-Nd mantle array: crustal extraction vs. recycling by subduction. Earth Planet. Sci. Lett. 530, 115941.
Johnston, S., Brandon, A., McLeod, C., Rankenburg, K., Becker, H., Copeland, P., 2022. Nd isotope variation between the Earth–Moon system and enstatite chondrites. Nature 611 (7936), 501–506.
Kemp, A.I.S., Hawkesworth, C.J., 2014. Growth and differentiation of the continental crust from isotope studies of accessory minerals. In: Treatise on Geochemistry, second edition. Elsevier, pp. 379–421.
Kemp, A.I., Hickman, A.H., Kirkland, C.L., Vervoort, J.D., 2015. Hf isotopes in detrital and inherited zircons of the Pilbara Craton provide no evidence for Hadean continents. Precambrian Res. 261, 112–126.
Kemp, A.I., Whitehouse, M.J., Vervoort, J.D., 2019. Deciphering the zircon Hf isotope systematics of Eoarchean gneisses from Greenland: implications for ancient crust-mantle differentiation and Pb isotope controversies. Geochim. Cosmochim. Acta 250, 76–97.
Kemp, A.I.S., Vervoort, J.D., Petersson, A., Smithies, R.H., Lu, Y., 2023. A linked evolution for granite-greenstone terranes of the Pilbara Craton from Nd and Hf isotopes, with implications for Archean continental growth. Earth Planet. Sci. Lett. 601, 117895.
Kitajima, K., Ushikubo, T., Kita, N.T., Maruyama, S., Valley, J.W., 2012. Relative retention of trace element and oxygen isotope ratios in zircon from Archean rhyolite, Panorama formation, North Pole Dome, Pilbara Craton, western Australia. Chem. Geol. 332, 102–115.
Luais, B., de Veslud, C.L.C., Géraud, Y., Gauthier-Lafaye, F., 2009. Comparative behavior of Sr, Nd and Hf isotopic systems during fluid-related deformation at middle crust levels. Geochim. Cosmochim. Acta 73 (10), 2961–2977.
McCulloch, M.T., 1987. Sm–Nd isotopic constraints on the evolution of Precambrian crust in the Australian continent. In: Proterozoic Lithospheric Evolution, pp. 115–130.
McCulloch, M.T., Black, L.P., 1984. SmNd isotopic systematics of Enderby Land granulites and evidence for the redistribution of Sm and Nd during metamorphism. Earth Planet. Sci. Lett. 71, 46–58.
Meintzer, R.E., Mitchell, R.S., 1988. The epigene alteration of allanite. Can. Mineral. 26 (4), 945–955.
Moecher, D.P., Perkins III, D., Leier-Englehardt, P.J., Medaris Jr, L.G., 1986. Metamorphic conditions of late archean high-grade gneisses, Minnesota river valley, USA. Can. J. Earth Sci. 23 (5), 633–645.
Morin, J.A., 1977. Allanite in granitic rocks of the Kenora-Vermilion Bay area, northwestern Ontario. Can. Mineral. 15, 297–302.
Murphy, D., Rizo, H., O'Neil, J., Hepple, R., Wiemer, D., Kemp, A., Vervoort, J., 2021. Combined Sm-Nd, Lu-Hf, and $^{142}$Nd study of paleoarchean basalts from the East Pilbara Terrane, western Australia. Chem. Geol. 578, 120301.
McNaughton, N.J., Compston, W., Barley, M.E., 1993. Constraints on the age of the Warrawoona group, eastern Pilbara Block, western Australia. Precambrian Res. 60 (1–4), 69–98.
Petersson, A., Kemp, A.I., Hickman, A.H., Whitehouse, M.J., Martin, L., Gray, C.M., 2019a. A new 3.59 Ga magmatic suite and a chondritic source to the East Pilbara Craton. Chem. Geol. 511, 51–70.
Petersson, A., Kemp, A.I., Whitehouse, M.J., 2019b. A Yilgarn seed to the Pilbara Craton? Evidence from inherited zircons. Geology 47 (11), 1098–1102.
Petersson, A., Kemp, A.I., Gray, C.M., Whitehouse, M.J., 2020. Formation of early archean Granite-Greenstone Terranes from a globally chondritic mantle: insights from igneous rocks of the Pilbara Craton, western Australia. Chem. Geol. 551, 119757.

Rasmussen, B., 2000. Filamentous microfossils in a 3,235-million-year-old volcanogenic massive sulphide deposit. Nature 405 (6787), 676–679.
Rasmussen, B., Buick, R., 2000. Oily old ores: evidence for hydrothermal petroleum generation in an Archean volcanogenic massive sulfide deposit. Geology 28 (8), 731–734.
Rizo, H., Boyet, M., Blichert-Toft, J., Rosing, M., 2011. Combined Nd and Hf isotope evidence for deep-seated source of Isua lavas. Earth Planet. Sci. Lett. 312 (3–4), 267–279.
Salerno, R., Vervoort, J., Fisher, C., Kemp, A., Roberts, N., 2021. The coupled Hf-Nd isotope record of the early Earth in the Pilbara Craton. Earth Planet. Sci. Lett. 572, 117139.
Scherer, E.E., Cameron, K.L., Blichert-Toft, J., 2000. Lu–Hf garnet geochronology: closure temperature relative to the Sm–Nd system and the effects of trace mineral inclusions. Geochim. Cosmochim. Acta 64 (19), 3413–3432.
Schoene, B., Dudas, F.O., Bowring, S.A., De Wit, M., 2009. Sm–Nd isotopic mapping of lithospheric growth and stabilization in the eastern Kaapvaal craton. Terra Nova 21 (3), 219–228.
Smye, A.J., Marsh, J.H., Vermeesch, P., Garber, J.M., Stockli, D.F., 2018. Applications and limitations of U-Pb thermochronology to middle and lower crustal thermal histories. Chem. Geol. 494, 1–18.
Taylor, R., Clark, C., Reddy, S.M., 2012. The effect of grain orientation on secondary ion mass spectrometry (SIMS) analysis of rutile. Chem. Geol. 300, 81–87.
Wang, D., Shirey, S.B., Carlson, R.W., Fisher, C.M., Kemp, A.I., Bickford, M.E., 2022. Comparative Sm-Nd isotope behavior of accessory minerals: reconstructing the Sm-Nd isotope evolution of early Archean rocks. Geochim. Cosmochim. Acta 318, 190–212.
Valley, J.W., Lackey, J.S., Cavosie, A.J., Clechenko, C.C., Spicuzza, M.J., Basei, M.A.S., Bindeman, I.N., Ferreira, V.P., Sial, A.N., King, E.M., Peck, W.H., 2005. 4.4 billion years of crustal maturation: oxygen isotope ratios of magmatic zircon. Contrib. Mineral. Petrol. 150, 561–580.
Van Kranendonk, M.J., Kirkland, C.L., Cliff, J., 2015. Oxygen isotopes in Pilbara Craton zircons support a global increase in crustal recycling at 3.2 Ga. Lithos 228, 90–98.
Vervoort, J.D., Patchett, P.J., Gehrels, G.E., Nutman, A.P., 1996. Constraints on early Earth differentiation from hafnium and neodymium isotopes. Nature 379 (6566), 624–627.
Vervoort, J.D., Plank, T., Prytulak, J., 2011. The Hf–Nd isotopic composition of marine sediments. Geochim. Cosmochim. Acta 75 (20), 5903–5926.
Whitehouse, M.J., Kamber, B.S., 2005. Assigning dates to thin gneissic veins in high-grade metamorphic terranes: a cautionary tale from Akilia, southwest Greenland. J. Petrol. 46, 291–318.
Whitehouse, M.J., Kamber, B.S., Moorbath, S., 1999. Age significance of U–Th–Pb zircon data from early Archaean rocks of West Greenland—a reassessment based on combined ion-microprobe and imaging studies. Chem. Geol. 160, 201–224.
Zegers, T.E., Wijbrans, J.R., White, S.H., 1999. 40Ar/39Ar age constraints on tectonothermal events in the Shaw area of the eastern Pilbara granite–greenstone terrain (W Australia): 700 Ma of Archean tectonic evolution. Tectonophysics 311 (1–4), 45–81.
Zeh, A., Gerdes, A., Millonig, L., 2011. Hafnium isotope record of the Ancient Gneiss Complex, Swaziland, southern Africa: evidence for Archaean crust–mantle formation and crust reworking between 3.66 and 2.73 Ga. J. Geol. Soc. 168 (4), 953–964.